



# Crystallization kinetics of PCL and PCL–glass composites for additive manufacturing

Liliana Sofia Oliveira Pires<sup>1,2,3</sup> · Maria Helena Figueira Vaz Fernandes<sup>1,2</sup> · José Martinho Marques de Oliveira<sup>2,3</sup>

Received: 9 January 2018 / Accepted: 14 April 2018 / Published online: 24 April 2018  
© Akadémiai Kiadó, Budapest, Hungary 2018

## Abstract

The non-isothermal crystallization kinetics of polycaprolactone (PCL) and PCL–glass composites, used in fused filament fabrication (FFF), was investigated. Films of PCL and PCL reinforced with powders of a bioactive glass, from the CaO-P<sub>2</sub>O<sub>5</sub>-MgO-SiO<sub>2</sub> system, were prepared by solvent casting process. Crystal structure of the samples was examined by X-ray diffraction (XRD), and thermal properties were assessed by differential scanning calorimetry (DSC), at different cooling rates (5, 10, 15 and 20 °C min<sup>-1</sup>). The DSC curves of non-isothermal crystallization showed a significant dependence of crystallinity ( $X_c$ ) on the cooling rate. The relevant crystallization kinetic parameters were determined from DSC traces applying a combination of Avrami and Ozawa methods (Mo's method), Jeziorny method and Friedman method. It was observed that the presence of inorganic particles within the polymeric matrix clearly influenced the composite crystallization. The addition of glass particles allowed a decrease in  $X_c$  and accelerated the PCL crystallization rate. The slower cooling rates tested proved to be suitable for the biofabrication of PCL–glass composites by FFF techniques.

**Keywords** DSC · Biomaterials · Composites · Crystallization kinetics · Fused filament fabrication (FFF)

## Introduction

Tissue engineering has achieved a high standard of development pushing the research to new methods and technologies for assisting regenerative medicine. The main tissue engineering strategy involves the seeding of cells onto 3D porous structures, or scaffolds that are then placed with appropriate growth factors in bioreactors in order to stimulate cells proliferation and differentiation. With the aim of keeping its integrity and helping in the production of

the new tissues, scaffolds should have suitable design and strength [1, 2]. Drawbacks such as design restrictions, incapacity of accurately control macro- and micro-features as well as reproducibility problems can be successfully overcome with the use of additive manufacturing techniques [3–5]. The progress of tissue engineering within the new paradigm of regenerative medicine relies on the development of new composite materials fabricated by innovative techniques. In this context, the production of polymeric composites reinforced with bioactive glasses suitable for biofabrication through a technique such as fused filament fabrication (FFF) appears as a quite promising strategy for the development of customized implants, designed for each particular situation [6–9]. Among the various Federal Drug Administration (FDA) approved polymers suitable for FFF manufacturing, PCL has been reported as very promising due to its low melting temperature and viscoelastic properties. PCL is a semicrystalline biomaterial with a melting point (59–64 °C) that allows the control and manufacture of free forms, stimulating the research and application in tissue engineering [5, 10–16]. Few papers are referred in the

✉ Liliana Sofia Oliveira Pires  
liliana.pires@ua.pt

<sup>1</sup> Department of Materials and Ceramic Engineering, University of Aveiro, Campus Universitário de Santiago, 3810-193 Aveiro, Portugal

<sup>2</sup> CICECO - Aveiro Institute of Materials, University of Aveiro, Campus Universitário de Santiago, 3810-193 Aveiro, Portugal

<sup>3</sup> School of Design, Management and Production Technologies Northern Aveiro, University of Aveiro, Estrada do Cercal, n°449, 3720-509 Santiago de Riba-Ul, Oliveira de Azeméis, Portugal

literature on the biofabrication of PCL–glass composites [17–20].

The FFF technique uses thermoplastic-based materials to fabricate 3D models. The plastic filament is heated, selectively extruded and deposited layer by layer. In biofabrication of scaffolds PCL, polypropylene (PP), PCL–hydroxyapatite composites and PP–tricalcium phosphate composites are frequently used [7, 8, 21, 22]. The filling of PCL with calcium phosphate particles is expected to improve the composite bioactivity without compromising the stability required for bone formation [23]. The control of interconnected porosity is essential to allow the proper mass transport of oxygen and nutrients improving the cell growth and proliferation as confirmed with PP–tricalcium phosphate composite scaffolds [8].

During the biofabrication by FFF, the maximum heating temperature can reach 90 °C, and thus during the processing of PCL composites loaded with ceramic or glass particles, no chemical changes are expected in the inorganic material, particularly in the glasses, for which the transition temperature is much higher than 90 °C [24]. At these temperatures, physical/chemical changes will mainly occur, in the PCL, affecting in particular its crystallization. The study of PCL crystallization kinetics is thus of major importance for the understanding of the composites thermal behavior.

There are some articles reporting crystallization studies of PCL composites [25–31]. However, the crystallization behavior of PCL–glass composites under non-isothermal conditions is scarcely documented and far from being understood. In fact reports on the fabrication and characterization of PCL-based composites filled with inorganic particles are very recent [32].

Regarding the inorganic filler, it is well known that its nature and composition affect the composite bioactivity behavior being the glass particles usually more reactive than glass-ceramic particles. The presence of crystalline phases in the glass-ceramic usually decreases the kinetics of formation of the apatite layer responsible for bioactivity, which is associated with the lower amount of remaining glass matrix, available for dissolution and surface reactivity [33–35].

In the context of the development of new materials for tissue engineering applications, the comprehension of all these issues arises as very important.

This paper is focused on the study of crystallization kinetics of PCL and PCL–glass composites, to be used in FFF. The main objectives are: (1) to identify the physical/chemical changes in the PCL during thermal treatment and; (2) to assess the kinetics of the involved reactions aiming to control the crystallization process of PCL and PCL–glass composites and to shed light onto the biofabrication by FFF of scaffolds from those composites.

## Experimental

### Preparation of materials

PCL with average molar mass  $M_n = 45.000$  in the form of pellets was purchased from Sigma-Aldrich. PCL–glass composites were prepared by mixing PCL with 30 mass% of glass particles from the  $\text{CaO}\cdot\text{P}_2\text{O}_5\cdot\text{MgO}\cdot\text{SiO}_2$  system (designated by V7) with composition  $33.26\text{CaO}-28.07\text{P}_2\text{O}_5-23.03\text{SiO}_2-15.64\text{MgO}$  (mass%) and previously confirming in vitro bioactivity [36, 37]. Films of PCL and PCL-based composites reinforced with glass powders, with a mean particle size of 62  $\mu\text{m}$ , were prepared by solvent casting process.

### Characterization

Crystal structure of PCL and PCL-V7 composites was examined by XRD in a Rigaku Geigerflex DMax-C X-ray diffractometer with  $\text{CuK}\alpha$  radiation.

The thermal behavior of PCL and PCL-V7 composites was studied by DSC in a Shimadzu DSC-60 equipment, calibrated with standard indium, in air atmosphere. Samples of approximately 10 mg were encapsulated into standard aluminum pans. Then, the samples were heated from  $-80$  to  $90$  °C at  $20$  °C  $\text{min}^{-1}$  and kept at  $90$  °C for 5 min to eliminate the previous thermal history. After each program, the samples were heated again from  $-80$  to  $90$  °C at four different heating rates ( $\varphi_h = 5, 10, 15$  and  $20$  °C  $\text{min}^{-1}$ ) and cooled down to  $-80$  °C at cooling rates ( $\varphi$ ) of  $5, 10, 15$  and  $20$  °C  $\text{min}^{-1}$ , respectively. PCL and PCL-V7 composites were analyzed by scanning electron microscopy (SEM) by Hitachi, Model SU-70 and by reflected-light microscope (Nikon Eclipse L150).

### Non-isothermal crystallization kinetics

From the recorded DSC curves, it is possible to identify the points “start crystallization temperature” ( $T_0$ ), “end crystallization temperature” ( $T_c$ ), “crystallization peak temperature” ( $T_p$ ) and to determine the crystallization enthalpy (non-isothermal) ( $\Delta H_c$ ), by integrating the area under the exothermic curve.

The crystallinity ( $X_c$ ) for PCL was calculated using the equation:

$$X_c = \frac{\Delta H_c}{\Delta H_f^0(1 - mf)} \times 100 \quad (1)$$

where  $\Delta H_f^0$  is the heat of fusion of 100% crystalline PCL ( $139.5$  J  $\text{g}^{-1}$ ) [25],  $\Delta H_c$  is the crystallization enthalpy, and  $mf$  is the mass glass fraction in the composite [38].

The relative degree of crystallinity ( $X_t$ ) as a function of temperature was obtained from the non-isothermal curve by integration:

$$X_t = \frac{\int_{T_0}^T \left(\frac{dH_c}{dT}\right) dT}{\int_0^\infty \left(\frac{dH_c}{dT}\right) dT} \quad (2)$$

taking  $dH_c/dT$  as the heat flow at temperature  $T$  [26, 39].

The half-time crystallization ( $t_{1/2}$ ) can be identified as the time taken to reach the value of 50% of relative crystallinity. This value gives an indication of the crystallization rate. The smaller the  $t_{1/2}$  value, the faster will be the crystallization rate.

Several models have been reported in the literature to describe non-isothermal crystallization. Theoretical approach based on modified Avrami equations is the most applied. The kinetic parameters of non-isothermal crystallization were determined based on the combination of Avrami and Ozawa equations (Mo's method), Jeziorny equation and Friedman equation [26, 40–46].

The Avrami equation [40, 44, 47, 48], commonly used in isothermal conditions, expresses the time dependence of the relative degree of crystallinity through the relationship:

$$X_t = 1 - \exp(-Z_t t^n) \quad (3)$$

or

$$\log[-\ln(1 - X_t)] = \log Z_t + n \log t \quad (4)$$

where  $t$  is the time taken by the crystallization process,  $n$  is the Avrami crystallization exponent, related to nucleation and growth mechanisms, and  $Z_t$  is a crystallization rate constant.

Jeziorny proposed a modified Avrami equation to analyze non-isothermal crystallization kinetics [45, 49]. As the temperature is not constant, Avrami parameters ( $n$  and  $Z_t$ ) do not have the same physical meaning as in the isothermal crystallization processes. For non-isothermal crystallization process, it is necessary to consider the effect of heating rate. To reflect the temperature dependence [26], the  $Z_t$  parameter in Eq. (3) should be rectified to  $Z_c$  by Jeziorny method [39, 45, 49–51] through the following equation:

$$\log Z_c = \frac{\log Z_t}{\varphi} \quad (5)$$

Ozawa equation [43] is used as an extension of the Avrami equation to describe the non-isothermal crystallization. This equation is one of the most used models to analyze non-isothermal crystallization kinetics. Assuming that the non-isothermal crystallization process is composed of infinitesimally small isothermal crystallization steps, the relationship between  $X_t$  and temperature can be expressed as follows:

$$X_t = 1 - \exp\left[-\frac{K(T)}{\varphi^m}\right] \quad (6)$$

or

$$\log[-\ln(1 - X_t)] = \log K(T) + m \log \varphi^{-1} \quad (7)$$

where  $m$  is the Ozawa exponent, which depends on the crystal growth and nucleation mechanism,  $\varphi$  is the cooling rate,  $K(T)$  is the crystallization rate constant, and  $m$  is the Ozawa crystallization exponent. The above equations cannot adequately describe the full process of non-isothermal crystallization of polymers in general. When the cooling rates vary in a large range, the results may not fit the linear representation described by Eq. (6). Huang et al. [26] reported that the crystallization of PCL and its composites is a complicated process and can affect the application of the Ozawa equation.

The combination of Avrami and Ozawa equations (Mo's method) [42] was proposed to describe the non-isothermal crystallization process [40, 51, 52]. A relationship between  $\varphi$  and  $t$  is expressed as follows:

$$\log \varphi = \log F(T) - \alpha \log t \quad (8)$$

where  $F(T)$  is the crystallization rate parameter and  $\alpha$  ( $\alpha = n/m$ ) is the ratio of the Avrami and Ozawa exponents,  $n$  and  $m$ , respectively. Plotting  $\log \varphi$  as a function of  $\log t$ , at a given degree of crystallinity, a straight line should be obtained. From the slope and intercept of lines, the  $-\alpha$  and the  $\log F(T)$  values are determined. The relationship between time and temperature can be defined from the following equation:

$$t = \frac{T_0 - T}{|\varphi|} \quad (9)$$

where  $T_0$  is the start crystallization temperature,  $T$  is the temperature at crystallization time  $t$ , and  $\varphi$  is the cooling rate.

The Kissinger equation has also been applied to describe the non-isothermal crystallization process [40, 41, 53]. From this method, the crystallization activation energy can be calculated but is mathematically unappropriated for crystallization studies with cooling experiments [54]. According to some researches [15, 55, 56], the isoconversional method of Friedman [57] revealed to be more valid and it was applied on this investigation.

The relationship between the crystallization activation energy ( $E_c$ ) and  $X_t$  was determined by Friedman equation:

$$\ln\left(\frac{d\alpha}{dt}\right) = \ln(Af(\alpha)) - \frac{E_c}{R} \quad (10)$$

where  $d\alpha/dt$  is the instantaneous crystallization rate as a function of time,  $A$  is the frequency factor,  $f(\alpha)$  is a function of conversion, and  $R$  is the gas constant. From degrees of

crystallinity (0.1–0.9), the values of  $dx/dt$  at a specific  $\alpha$  are correlated with the corresponding crystallization temperature at this  $\alpha$ . The slope of the plot  $-\ln(dx/dt)$  versus  $(1/T) \times 10^3$  gives the value of  $E_c$ , and the dependency of  $E_c$  and  $X_t$  is evaluated.

## Results and discussion

### Structural properties

The presence of crystalline phases in the glass-free PCL and in the PCL–glass composite was investigated by XRD. Figure 1 shows peaks with significant intensity at  $2\theta = 21.4^\circ$  for the diffraction of the (110) plane,  $2\theta = 22^\circ$  for the (111) plane and  $2\theta = 23.8^\circ$  for the (200) plane. These peaks are according to the results reported by other researchers [58–60], indicating the presence of crystalline phases (poly- $\epsilon$ -caprolactone), together with other less intense peaks also attributed to Poly- $\epsilon$ -caprolactone.

The XRD plot of the PCL-V7 film is representative of a structure that is mainly amorphous with very incipient crystallization at the same peaks  $2\theta = 21.4^\circ$  and  $2\theta = 23.8^\circ$ . This indicates that the addition of 30 mass% glass inhibits the occurrence of crystallization within the polymeric matrix.

SEM micrographs in Fig. 2a, c clearly show the typical spherulitic morphology of the neat polymer and the homogeneously dispersed glass particles within the polymeric matrix of the composite. It is reported in the literature that the size of PCL spherulites may be affected by the presence of a filler, as observed by Liu et al. [58] in PCL–calcium sulfate whisker composites where there was a grain refining effect of the filler on the matrix. This is compared with neat PCL. In micrographs obtained by optical microscopy (Fig. 2b, d), the effect of glass particles on PCL crystallization is more evident. The PCL-V7

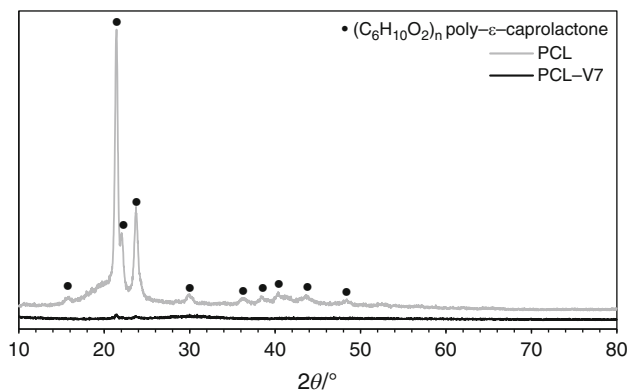


**Fig. 1** XRD analysis of the PCL and PCL-V7 films prepared by solvent casting

composite presents a large number of spherulites with smaller dimensions, revealing the nucleating ability of glass particles.

### Thermal properties

For non-isothermal crystallization of PCL and PCL-V7 composites, the samples were heated in the DSC equipment to allow melting of the polymer crystals (endothermic peak) and then cooled to study the crystallization of the samples (exothermic crystallization peaks). Figure 3 shows typical DSC curves of PCL and PCL-V7 composites when heating and cooling at the same rate of  $15\text{ }^\circ\text{C min}^{-1}$ .

The DSC curves for all samples heated and then cooled at 5, 10, 15 and  $20\text{ }^\circ\text{C min}^{-1}$  are shown in Fig. 4. An increase in enthalpy with the increase in cooling rate is observed. As reported in the literature for some polymeric composites [25, 55, 61] and for PCL [15, 25, 62–64], this kind of variation is associated with the intrinsic non-isothermal crystallization process of PCL that leads to the development of imperfect crystals at higher cooling rates. A similar trend was observed by Huang et al. [26], in a study on the non-isothermal crystallization of modified bamboo fiber–PCL composites.

Table 1 presents the relevant crystallization parameters taken from the DSC curves, including the peak crystallization temperature ( $T_p$ ), the starting crystallization temperature ( $T_0$ ), the end crystallization temperature ( $T_c$ ) and other information such as the crystallinity ( $X_c$ ), the crystallization enthalpy ( $\Delta H_c$ ) and the half-time crystallization ( $t_{1/2}$ ), calculated from Eqs. (1) and (2).

The results of  $T_p$  as a function of the cooling rate (Fig. 5a) show that for both neat PCL and PCL-V7 composite the increase in the cooling rates delays the crystallization, pushing the peak temperatures for lower values. A similar behavior was observed in neat PCL, in PCL–poly(ethylene glycol)–PCL triblock copolymer, in starch–PCL and in composites with an inorganic filler [25, 55, 64, 65]. This means that when cooling at  $5\text{ }^\circ\text{C min}^{-1}$  the maximum crystallization rate (at  $T_p$ ) is achieved sooner at higher temperatures (and thus  $T_p$  appears at a higher value on cooling). For the faster cooling rates, lower temperatures will be required to produce the chains reorganization within the polymeric matrix, with  $T_p$  occurring later, i.e., at lower values [15].

The trend of the  $T_p$  values for the PCL-V7 composites also suggests that on cooling in the DSC equipment the glass particles in the PCL matrix promote a crystallization that occurs earlier (i.e., at higher temperatures) compared with the neat PCL.

Regarding the relationship between the cooling rates and the crystallinity,  $X_c$ , different indications are given for the neat PCL and for the composite (Fig. 5b).  $X_c$  values are

**Fig. 2** Surface SEM and optical micrographs. PCL: **a** SEM and **b** optical microscopy. PCL-V7: **c** SEM and **d** optical microscopy

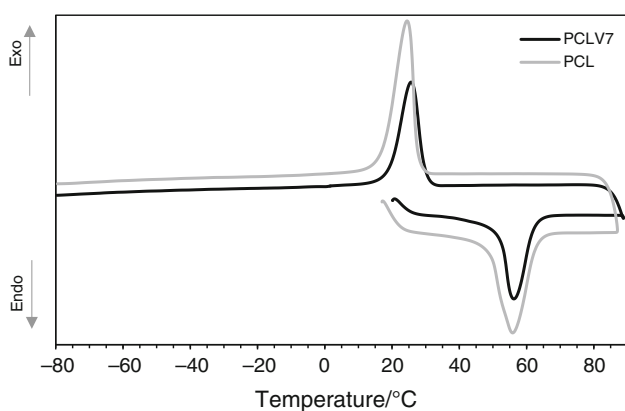
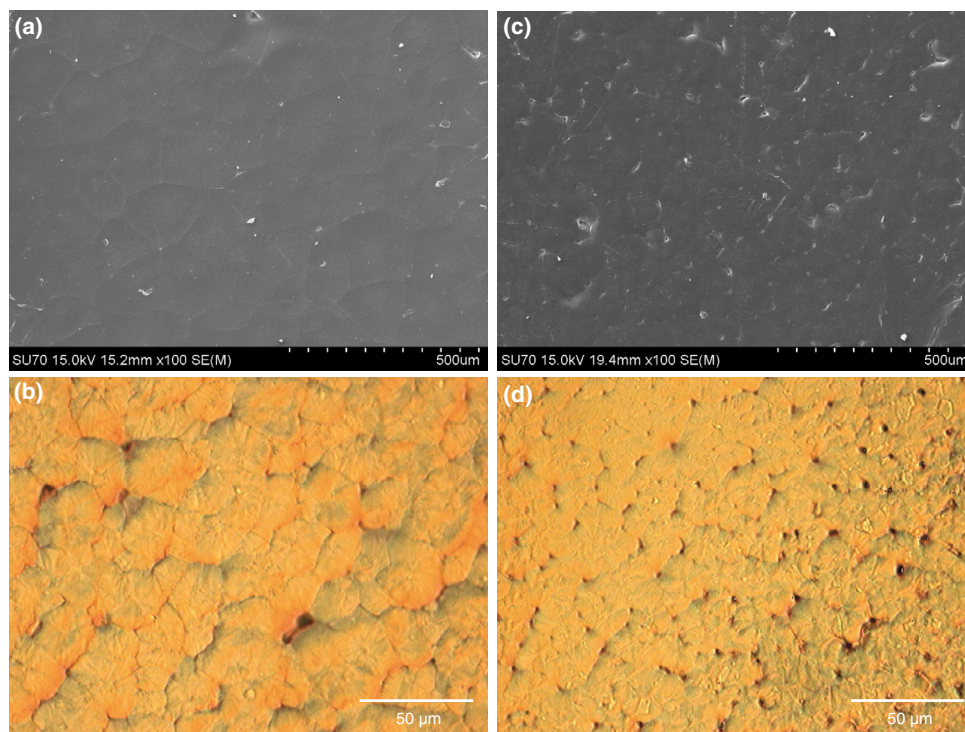


**Fig. 3** DSC curves of PCL and PCL-V7 composites on heating and on cooling at the same rates of  $15\text{ }^{\circ}\text{C min}^{-1}$

much lower for the PCL-V7 composite than for the PCL alone, and in each case the variation of crystallinity with cooling rates has different trends.

In the glass-free PCL, for example, 49% of crystallinity is attained by cooling the samples at  $5\text{ }^{\circ}\text{C min}^{-1}$ . Doubling the cooling rate to  $10\text{ }^{\circ}\text{C min}^{-1}$  produces an increase in the crystallinity to 54%, a value that is approximately maintained, independently of the rates at which samples are cooled. For the PCL-V7 composite, the results show a gradual increase of  $X_c$  with the increase in cooling rates, with all crystallinity values well below the ones obtained with the unfilled PCL samples. It is suggested that the presence of the glass particles (30% in mass) may hinder

the mobility and rearrangement of the polymer chains, thus preventing the crystallization of the PCL fraction. At the temperatures at which the thermal analysis is carried out (below  $90\text{ }^{\circ}\text{C}$ ), the only expected modifications refer to the PCL fraction and not to the glass particles that should remain amorphous and without morphological changes.

It is reported in the literature [66] that in PCL–bioglass composites the crystallinity  $X_c$  was lower in the composite than in the neat PCL, a behavior that was attributed to interface interactions between the filler and the matrix. Cesur et al. [60] studied the crystallization kinetics of PCL with some inorganic additives (e.g., zinc oxide, organoclay and hydroxiapatite) and found that for small amounts, the additives acted as nucleating agents, increasing the crystallinity. However, in high concentration, these additives prevented the movement of polymer molecules and a lower crystallinity was observed. The nucleating role of sisal fiber in a PCL composite was also reported by Carmona et al. [67] that observed a crystallinity increase in the PCL fraction due to the presence of the filler.

The plots of relative degree of crystallinity as a function of temperature or time (Fig. 6) provide equivalent information. The crystallization process starts at higher temperatures for the slower cooling rates (e.g.,  $5\text{ }^{\circ}\text{C min}^{-1}$ ), and it occurs during a longer period of time. Although the crystallization process begins at lower temperatures at the higher cooling rates (e.g.,  $20\text{ }^{\circ}\text{C min}^{-1}$ ), the duration time is shorter. In the case of PCL, less time is required to obtain a specific value of relative degree of crystallinity, proving

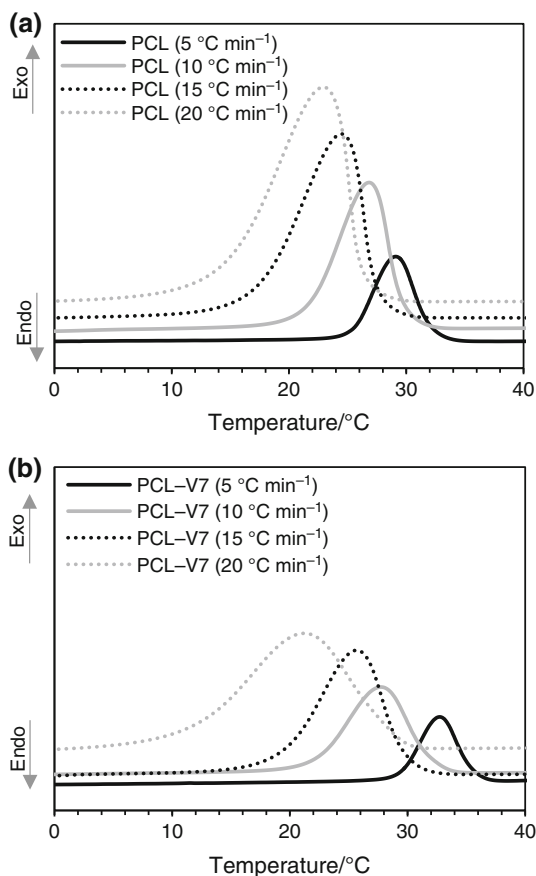


**Fig. 4** DSC curves of non-isothermal crystallization of **a** PCL and **b** PCL-V7 composites at cooling rates of 5, 10, 15 and 20 °C min<sup>-1</sup>

also that the shorter crystallization time was obtained at faster cooling rates, similarly to what is reported in the literature [15]. In the case of PCL-V7, it was observed that a shorter crystallization time also corresponds to the faster cooling rates with no significant differences in the crystallinities obtained at 15 and 20 °C min<sup>-1</sup>. These results are in agreement with the indications from  $t_{1/2}$  values in Table 1, where the faster crystallization rates correspond to the smaller  $t_{1/2}$  values.

**Table 1** Non-isothermal crystallization of PCL and PCL-V7 composites relevant parameters taken from DSC curves

Samples	$\phi/^\circ\text{C min}^{-1}$	$T_0/^\circ\text{C}$	$T_c/^\circ\text{C}$	$T_p/^\circ\text{C}$	$\Delta H_c/\text{J g}^{-1}$	$X_c/\%$	$t_{1/2}/\text{s}$
PCL	5	34.84	21.94	29.46	68.42	49.05	71
	10	33.37	13.78	26.95	75.74	54.29	43
	15	31.53	5.04	24.73	74.71	53.56	33
	20	30.50	1.11	23.12	76.61	54.92	28
PCL-V7	5	37.97	25.84	32.89	44.87	22.52	65
	10	34.46	15.42	28.16	51.59	25.89	43
	15	33.35	12.44	25.72	57.60	28.9	35
	20	32.98	2.309	22.99	60.84	32.03	33

$\phi$ —cooling rate;  $T_0$ —starting crystallization temperature;  $T_c$ —end crystallization temperature;  $T_p$ —peak crystallization temperature;  $\Delta H_c$ —crystallization enthalpy;  $X_c$ —crystallinity;  $t_{1/2}$ —half-time crystallization

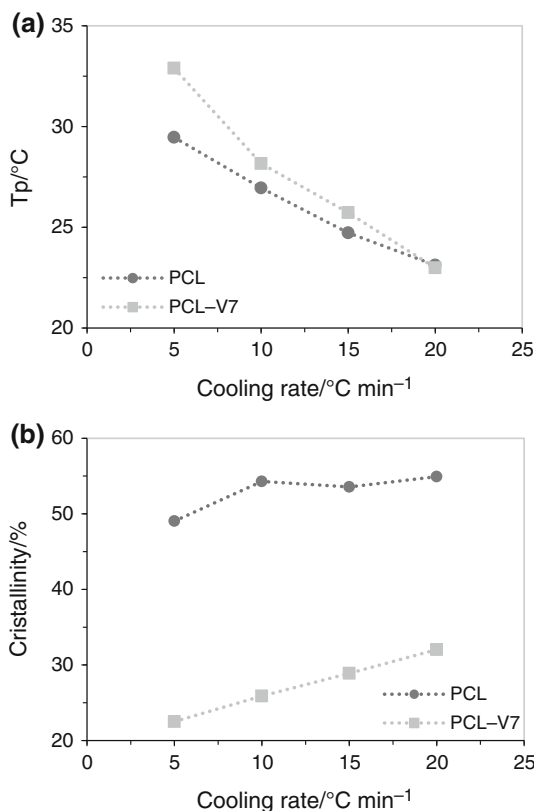


**Fig. 5** Crystallization peak temperature  $T_p$  (a) and crystallinity  $X_c$  (b) as a function of cooling rate of PCL and PCL-V7 composites

**Non-isothermal crystallization kinetics**

In isothermal crystallization of polymers, Avrami model gives reliable correlations but in non-isothermal crystallization the Avrami kinetic parameters  $n$  and  $Z_t$ , obtained from Fig. 7, do not have the same physical meaning because in these conditions, the nucleation and crystal growth processes are dependent on temperature [50].

In this study,  $X_t$  values were considered between 5 and 95%. The values of relevant kinetic parameters calculated from based on Avrami and Jeziorny method are depicted in

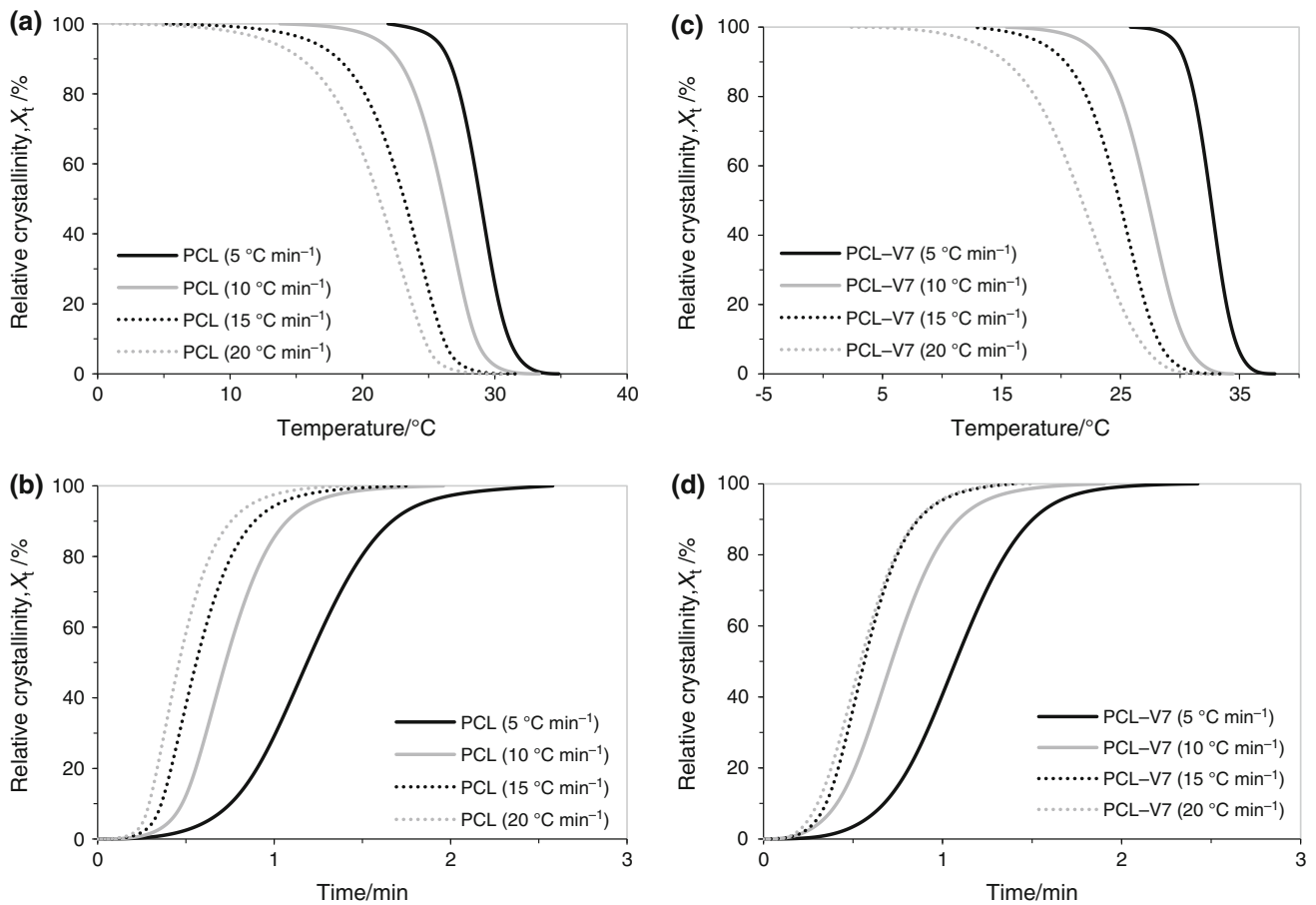


**Fig. 6** Relative degree of crystallinity as a function of temperature and time for **(a, b)** neat PCL and **(c, d)** PCL-V7 composites

Table 2. As shown  $Z_c$  increases with increasing cooling rate, meaning a faster crystallization rate at higher cooling rates as reported in the literature [55, 64]. It is also evident that, for the same cooling rate, the crystallization rate is higher for the samples with glass particles than for the non-filled PCL.

The values of  $n$  between 3 and 4 for the neat PCL and for the composite samples suggest a three-dimensional spherulite growth with homogeneous nucleation for both cases, as also found by other authors working with the same polymeric matrix [26].

To obtain the kinetic parameters based on the Mo's method, the results for non-isothermal crystallization of PCL and PCL-V7 composites at four cooling rates are plotted in Fig. 8 as  $\text{Log } \varphi$  versus  $\text{Log } t$ . A good linearity is obtained for all situations [52]. From the slopes and the interceptions of these lines,  $\alpha$  and  $F(T)$  parameters can be calculated (Table 3). For both cases, unfilled and filled PCL, the values of  $\alpha$  and  $F(T)$  increase with the increase in relative degree of crystallinity. Being  $\alpha = n/m$  with  $n$  and  $m$  the Avrami and Ozawa exponents, respectively, this means that either for PCL or for PCL-V7 composites the Avrami exponent is lower than the Ozawa exponent and

that Avrami exponent increases faster than Ozawa exponent with increasing relative degree of crystallinity.  $F(T)$  indicates the polymer crystallization rate, a lower  $F(T)$  value meaning a higher crystallization rate [40, 42].

Comparing the values of  $F(T)$  for PCL and PCL-V7, it is seen that, for all degrees of crystallinity,  $F(T)$  is smaller for PCL-V7, meaning that crystallization rate in the composites is faster than in the PCL. The addition of glass particles accelerated the PCL crystallization rate in agreement with the results in Table 1 that show that on cooling  $T_p$  values for PCL-V7 are higher than for PCL, for the same cooling rate.

The presence of the glass as reinforcing filler can act as a nucleating agent, facilitating the formation and growth of spherulites within the PCL matrix [26].

The crystallization activation energy for the non-isothermal process  $E_c$  was evaluated by Friedman method (Eq. 10; Fig. 9). The straight lines of  $-\ln(d\alpha/dt)$  versus  $(1/T) \times 10^3$  plots allowed the calculation of the  $E_c$  at different degrees of crystallinity (coefficient of determination in linear regression  $R^2 = 0.95$ ). The dependence of  $E_c$  on  $X_t$  is illustrated in Fig. 9.

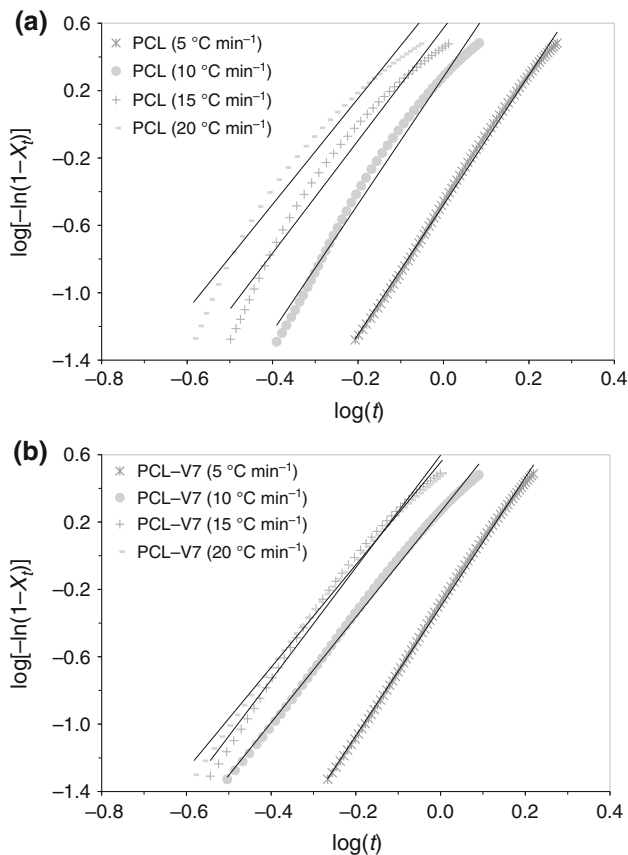


**Fig. 7** Plots of  $\log[-\ln(1-X_t)]$  and  $\log(t)$  for **a** neat PCL and **b** PCL-V7 composites

**Table 2** Non-isothermal crystallization kinetic parameters based on Avrami and Jeziorny methods

Samples	$\phi/^\circ\text{C min}^{-1}$	$n$	$Z_t/\text{min}^{-1}$	$Z_c/\text{min}^{-1}$	$r^2$
PCL	5	3.85	0.33	0.80	0.9979
	10	3.78	1.91	1.07	0.9867
	15	3.34	3.72	1.09	0.9738
	20	3.14	6.04	1.09	0.9703
PCL-V7	5	3.38	0.50	0.87	0.9988
	10	3.13	1.82	1.06	0.9976
	15	3.04	3.58	1.07	0.994
	20	3.33	3.95	1.10	0.9889

$\phi$ —cooling rate;  $n$ —Avrami crystallization exponent;  $Z_r$ —crystallization rate constant;  $Z_c$ — $Z_r$  calibrated by Jeziorny method;  $r^2$ —coefficient of determination in linear regression

The results here obtained for PCL from the Friedman method are similar to those acquired in similar studies [15, 55]. Activation energy values for PCL crystallization vary from  $-110$  to  $-49$   $\text{kJ mol}^{-1}$  in  $X_t$  the range from 10 to 90% and for PCL-V7;  $E_c$  varies from  $-79$  to  $-28$   $\text{kJ mol}^{-1}$  in the same  $X_t$  range. The negative values

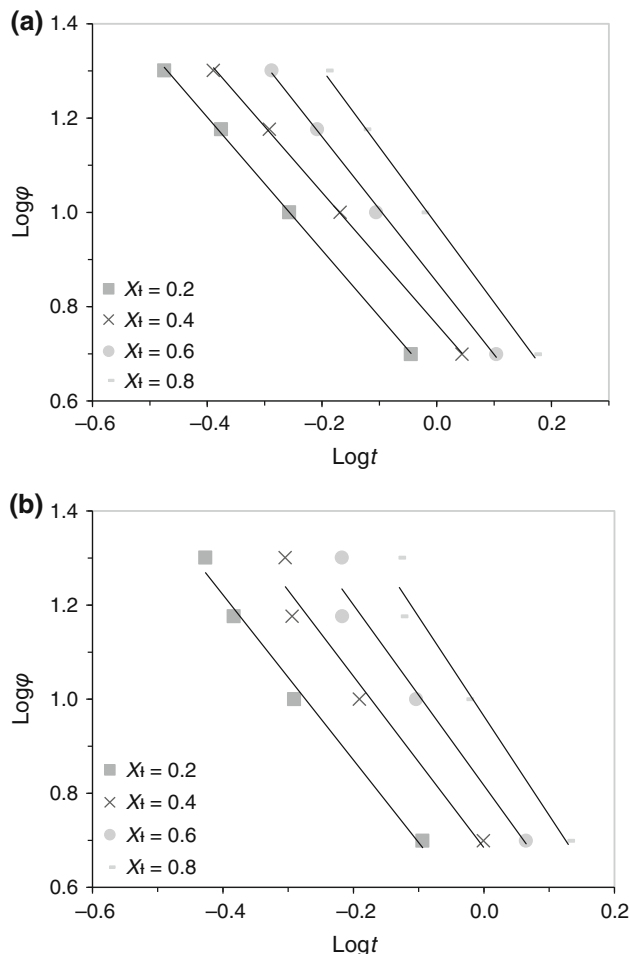


**Fig. 8** Plots of  $\log \phi$  as a function of  $\log t$  for **a** neat PCL and **b** PCL-V7 composites at various relative degrees of crystallinity  $X_t$

**Table 3** Non-isothermal crystallization kinetic parameters  $\alpha$  and  $F(T)$  based on Mo's method for different relative degrees of crystallinity  $X_t$

$X_t$	PCL			PCL-V7		
	$\alpha$	$F(T)$	$r^2$	$\alpha$	$F(T)$	$r^2$
0.2	1.41	4.34	0.9994	1.76	3.31	0.9882
0.4	1.40	5.79	0.9996	1.82	4.84	0.9961
0.6	1.54	7.12	0.9985	1.92	6.55	0.9608
0.8	1.65	9.41	0.9978	2.11	9.20	0.9641

$\alpha$ —ratio of the Avrami and Ozawa exponent;  $F(T)$ —crystallization rate parameter;  $r^2$ —coefficient of determination in linear regression

are indicative of the exothermic nature of the transition from melt to crystalline state [40]. For the PCL-V7 composite, the  $E_c$  values are higher than for neat PCL, indicating that the energy barrier for the melt-crystallization process is higher for the composite than for the unfilled PCL [50]. As reported for other crystallization studies



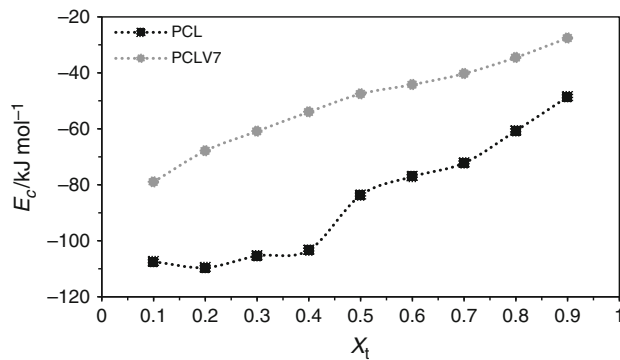


**Fig. 9** Plots of  $E_c$  (kJ mol<sup>-1</sup>) as a function of  $X_t$  for neat PCL and for PCL-V7 composites

[38, 40, 55], the presence of glass particles in the PCL-V7 composite should contribute for the observed difference in the activation energy values. It is likely that the V7 particles restrict the mobility of PCL chains and the development of crystallinity in PCL-V7. Thus, more energy is required to rearrange chains in the polymer fraction of the composite, comparing with the neat PCL [64].

## Conclusions

The study of non-isothermal crystallization of PCL and PCL-V7 glass composites carried out in a DSC equipment showed that there was a significant effect of the glass filler on the crystallization process.

The presence of the glass particles promoted a faster crystallization on cooling, with higher peak crystallization temperatures  $T_p$  in the PCL-V7 composites than in the unfilled PCL. Additionally, for the same cooling rate, the crystallinity  $X_c$  of the composites was lower than the one for the neat PCL. A minimum value of 23% of crystallinity was obtained for the composite PCL-V7 at 5 °C min<sup>-1</sup>. This means that during a biofabrication process to obtain PCL-V7 scaffolds slower cooling rates should be advisable to produce scaffolds with a less content of crystalline phases, a relevant parameter for the further control of the material's bioactivity.

The non-isothermal crystallization kinetics was analyzed by different models, namely the Mo's method, the Jeziorny method and the Friedman method. The models proved to be suitable for describing the undertaken non-isothermal studies.

This work revealed that it is possible to have a sensible knowledge of the relevant parameters governing the crystallization of an important polymer—PCL and a particular new composite—PCL-V7 glass with potential biomedical applications. Recent techniques for the manufacture of

scaffolds from these materials, such as FFF, may greatly profit from the set of information provided by these studies.

**Acknowledgements** This work was developed within the scope of the project CICECO-Aveiro Institute of Materials, POCI-01-0145-FEDER-007679 (FCT Ref. UID /CTM /50011/2013), financed by national funds through the FCT/MEC and when appropriate co-financed by European Regional Development Fund (FEDER) through the International and Competitive Operational Program (POCI) under the PT2020 Partnership Agreement.

## References

- Butscher A, Bohner M, Hofmann S, Gauckler L, Müller R. Structural and material approaches to bone tissue engineering in powder-based three-dimensional printing. *Acta Biomater.* 2011;7(3):907–20.
- Best SM, Porter AE, Thian ES, Huang J. Bioceramics: past, present and for the future. *J Eur Ceram Soc.* 2008;28(7):1319–27.
- Schlickewei W, Schlickewei C. The use of bone substitutes in the treatment of bone defects—the clinical view and history. *Macromol Symp.* 2007;253(1):10–23.
- Bergmann C, Lindner M, Zhang W, Koczur K, Kirsten A, Telle R, et al. 3D printing of bone substitute implants using calcium phosphate and bioactive glasses. *J Eur Ceram Soc.* 2010;30(12):2563–7.
- Woodruff MA, Hutmacher DW. The return of a forgotten polymer—polycaprolactone in the 21st century. *Prog Polym Sci.* 2010;35(10):1217–56.
- Hutmacher DW, Sittinger M, Risbud MV. Scaffold-based tissue engineering: rationale for computer-aided design and solid free-form fabrication systems. *Trends Biotechnol.* 2004;22(7):354–62.
- Zein I, Hutmacher DW, Tan KC, Teoh SH. Fused deposition modeling of novel scaffold architectures for tissue engineering applications. *Biomaterials.* 2002;23(4):1169–85.
- Kalita SJ, Susmita B, Hosick HL, Amit B. Development of controlled porosity polymer-ceramic composite scaffolds via fused deposition modeling. *Mater Sci Eng C.* 2003;23(5):10.
- Melchels FPW, Domingos MAN, Klein TJ, Malda J, Bartolo PJ, Hutmacher DW. Additive manufacturing of tissues and organs. *Prog Polym Sci.* 2012;37(8):1079–104.
- Ciardelli G, Chiono V, Vozzi G, Pracella M, Ahluwalia A, Barbani N, et al. Blends of poly( $\epsilon$ -caprolactone) and polysaccharides in tissue engineering applications. *Biomacromolecules.* 2005;6(4):1961–76.
- Papadimitriou SA, Papageorgiou GZ, Bikiaris DN. Crystallization and enzymatic degradation of novel poly( $\epsilon$ -caprolactone-co-propylene succinate) copolymers. *Eur Polym J.* 2008;44(7):2356–66.
- Vassiliou AA, Papageorgiou GZ, Achilias DS, Bikiaris DN. Non-isothermal crystallisation kinetics of in situ prepared poly( $\epsilon$ -caprolactone)/surface-treated SiO<sub>2</sub> nanocomposites. *Macromol Chem Phys.* 2007;208(4):364–76.
- Sanandaji N. Different paths to explore confined crystallisation of PCL. Stockholm: Royal Institute of Technology; 2013.
- Abedalwafa M, Wang F, Wang L, Li C. Biodegradable poly- $\epsilon$ -silicon-caprolactone (PCL) for tissue engineering applications: a review. *Rev Adv Mater Sci.* 2013;34:123–40.
- Limwanich W, Phetsuk S, Meepowpan P, Kungwan N, Punyodom W. Kinetics studies of non-isothermal melt crystallization of poly( $\epsilon$ -caprolactone) and poly(L-lactide). *Chiang Mai J Sci.* 2016;43(2):329–38.

16. Murphy SH, Leeke GA, Jenkins MJ. A Comparison of the use of FTIR spectroscopy with DSC in the characterisation of melting and crystallisation in polycaprolactone. *J Therm Anal Calorim.* 2012;107(2):669–74.
17. Zhang J, Zhao S, Zhu M, Zhu Y, Zhang Y, Liu Z, et al. 3D-printed magnetic Fe<sub>3</sub>O<sub>4</sub>/MBG/PCL composite scaffolds with multifunctionality of bone regeneration, local anticancer drug delivery and hyperthermia. *J Mater Chem B.* 2014;2(43):7583–95.
18. Poh PSP, Hutmacher DW, Stevens MM, Woodruff MA. Fabrication and in vitro characterization of bioactive glass composite scaffolds for bone regeneration. *Biofabrication.* 2013;5(4):45005.
19. Chia H, Wu B. Recent advances in 3D printing of biomaterials. *J Biol Eng.* 2015;9(1):1–14.
20. Bose S, Vahabzadeh S, Bandyopadhyay A. Bone tissue engineering using 3D printing. *Mater Today.* 2013;16(12):496–504.
21. Yao Q, Wei B, Guo Y, Jin C, Du X, Yan C, et al. Design, construction and mechanical testing of digital 3D anatomical data-based PCL–HA bone tissue engineering scaffold. *J Mater Sci Mater Med.* 2015;26(1):51.
22. Temple JP, Hutton DL, Hung BP, Huri PY, Cook CA, Kondragunta R, et al. Engineering anatomically shaped vascularized bone grafts with hASCs and 3D-printed PCL scaffolds. *J Biomed Mater Res Part A.* 2014;102(12):4317–25.
23. van Manen EHC, Zhang W, Walboomers XF, Vazquez B, Yang F, Ji W, et al. The influence of electrospun fibre scaffold orientation and nano-hydroxyapatite content on the development of tooth bud stem cells in vitro. *Odontology.* 2014;102(1):14–21.
24. Rodriguez G, Dias J, D'Ávila MA, Bártolo P. Influence of hydroxyapatite on extruded 3D scaffolds. *Procedia Eng.* 2013;59:263–9.
25. Wang Y, Rodriguez-Perez MA, Reis RL, Mano JF. Thermal and Thermomechanical Behaviour of Polycaprolactone and Starch/Polycaprolactone Blends for Biomedical Applications. *Macromol Mater Eng.* 2005;290(8):792–801.
26. Huang Y, Liu H, He P, Yuan L, Xiong H, Xu Y, et al. Non-isothermal crystallization kinetics of modified bamboo fiber/PCL composites. *J Appl Polym Sci.* 2010;116:2119–25.
27. Di Maio E, Iannace S, Sorrentino L, Nicolais L. Isothermal crystallization in PCL/clay nanocomposites investigated with thermal and rheometric methods. *Polymer (Guildf).* 2004;45(26):8893–900.
28. Hao J, Yuan M, Deng X. Biodegradable and biocompatible nanocomposites of poly( $\epsilon$ -caprolactone) with hydroxyapatite nanocrystals: thermal and mechanical properties. *J Appl Polym Sci.* 2002;86(3):676–83.
29. Qiao X, Li W, Sun K, Xu S, Chen X. Nonisothermal crystallization behaviors of silk-fibroin-fiber-reinforced poly( $\epsilon$ -caprolactone) biocomposites. *J Appl Polym Sci.* 2009;111(6):2908–16.
30. Lanfranchi M, Alvarez VA, Ludueña LN. Isothermal crystallization of polycaprolactone/modified clay biodegradable nanocomposites. *J Therm Anal Calorim.* 2016;126(3):1273–80.
31. Perez CJ, Vázquez A, Alvarez VA. Isothermal crystallization of layered silicate/starch-polycaprolactone blend nanocomposites. *J Therm Anal Calorim.* 2008;91(3):749–57.
32. Liang JZ, Zhou L, Tang CY, Tsui CP. Crystallization properties of polycaprolactone composites filled with nanometer calcium carbonate. *J Appl Polym Sci.* 2013;128(5):2940–4.
33. Clupper DC, Mecholsky JJ Jr, LaTorre GP, Greenspan DC. Bioactivity of tape cast and sintered bioactive glass-ceramic in simulated body fluid. *Biomaterials.* 2002;23(12):2599–606.
34. Chen QZ, Thompson ID, Boccaccini AR. 45S5 Bioglass<sup>®</sup>-derived glass-ceramic scaffolds for bone tissue engineering. *Biomaterials.* 2006;27(11):2414–25.
35. Guanabara PJ, Rodrigues ACM, Peitl O. Bioactivity study of glass-ceramics with various crystalline fractions obtained by controlled crystallization. *Mater Sci Eng. C.* 2004;24(5):689–91.
36. Oliveira JM, Correia RN, Fernandes M, Rocha J. Influence of the CaO/MgO ratio on the structure of phase-separated glasses: a solid state <sup>29</sup>Si and <sup>31</sup>P MAS NMR study. *J Non Cryst Solids.* 2000;265(3):221–9.
37. Gomes DF. Compósitos de PCL e vidro bioativo: estudo do comportamento in vitro. University of Aveiro; 2013.
38. Nath DCD, Bandyopadhyay S, Yu A, Blackburn D, White C. Novel observations on kinetics of nonisothermal crystallization in fly ash filled isotactic-polypropylene composites. *J Appl Polym Sci.* 2009;115(3):1510–7.
39. Şanlı S, Durmus A, Ercan N. Effect of nucleating agent on the nonisothermal crystallization kinetics of glass fiber- and mineral-filled polyamide-6 composites. *J Appl Polym Sci.* 2012;125(S1):E268–81.
40. Zhou WY, Duan B, Wang M, Cheung WL. Isothermal and non-isothermal crystallization kinetics of poly(L-Lactide)/carbonated hydroxyapatite nanocomposite microspheres. In: Dr. Boreddy Reddy, editor. *Advances in diverse industrial applications of nanocomposites.* InTech; 2011. p. 231–60.
41. Heireche L, Belhadji M. The methods matusita, kisinger and ozawa in the study of the crystallization of glasses. The case of Ge–Sb–Te alloys. *Chalcogenide Lett.* 2007;4(2):23–33.
42. Liu T, Mo Z, Wang S, Zhang H. Nonisothermal melt and cold crystallization kinetics of poly(aryl ether ether ketone ketone). *Polym Eng Sci.* 1997;37(3):568–75.
43. Ozawa T. Kinetics of non-isothermal crystallization. *Polymer (Guildf).* 1971;12(3):150–8.
44. Avrami M. Kinetics of phase change. II: transformation-time relations for random distribution of nuclei. *J Chem Phys.* 1940;8(2):212–24.
45. Shi N, Dou Q. Non-isothermal cold crystallization kinetics of poly(lactic acid)/poly(butylene adipate-co-terephthalate)/treated calcium carbonate composites. *J Therm Anal Calorim.* 2015;119(1):635–42.
46. Qiu S, Su Z, Qiu Z. Isothermal and nonisothermal crystallization kinetics of novel biobased poly(ethylene succinate-co-ethylene sebacate) copolymers from the amorphous state. *J Therm Anal Calorim.* 2017;129(2):801–8.
47. Patnaik KSKR, Devi KS, Kumar VK. Non-isothermal crystallization kinetics of polypropylene (PP) and polypropylene (PP)/talc nanocomposite. *Int J Chem Eng Appl.* 2010;1(4):346–53.
48. Shi XM, Zhang J, Jin J, Chen SJ. Non-isothermal crystallization and melting of ethylene-vinyl acetate copolymers with different vinyl acetate contents. *Express Polym Lett.* 2008;2(9):623–9.
49. Jeziorny A. Parameters characterizing the kinetics of the non-isothermal crystallization of poly(ethylene terephthalate) determined by d.s.c. *Polymer (Guildf).* 1978;19(10):1142–4.
50. Oburoğlu N, Ercan N, Durmus A, Kaşgöz A. Effects of filler type on the nonisothermal crystallization kinetics of poly(butylene terephthalate) (PBT) composites. *J Appl Polym Sci.* 2012;123(1):77–91.
51. Sun X, Mai K, Zhang C, Cao M, Zhang Y, Zhang X. Non-isothermal crystallization kinetics of bio-based semi-aromatic polyamides. *J Therm Anal Calorim.* 2017;130(2):1021–30.
52. Li Y, Han C, Yu Y, Xiao L, Shao Y. Isothermal and non-isothermal cold crystallization kinetics of poly(l-lactide)/functionalized eggshell powder composites. *J Therm Anal Calorim.* 2018;131(3):2213–23.
53. Saad GR, Elsawy MA, Aziz MSA. Nonisothermal crystallization behavior and molecular dynamics of poly(lactic acid) plasticized with jojoba oil. *J Therm Anal Calorim.* 2017;128(1):211–23.

54. Vyazovkin S, Burnham AK, Criado JM, Pérez-Maqueda LA, Popescu C, Sbirrazzuoli N. ICTAC Kinetics Committee recommendations for performing kinetic computations on thermal analysis data. *Thermochim Acta*. 2011;520(1–2):1–19.
55. Papageorgiou GZ, Achilias DS, Bikiaris DN, Karayannidis GP. Crystallization kinetics and nucleation activity of filler in polypropylene/surface-treated SiO<sub>2</sub> nanocomposites. *Thermochim Acta*. 2005;427(1–2):117–28.
56. Kang S-H, Ku D-C, Lim J-H, Yang Y-K, Kwak N-S, Hwang T-S. Characterization for pyrolysis of thermoplastic polyurethane by thermal analyses. *Macromol Res*. 2005;13(3):212–7.
57. Friedman HL. Kinetics of thermal degradation of char-forming plastics from thermogravimetry. Application to a phenolic plastic. *J Polym Sci Part C*. 1964;6:183–95.
58. Liu JY, Reni L, Wei Q, Wu JL, Liu S, Wang YJ, et al. Fabrication and characterization of polycaprolactone/calcium sulfate whisker composites. *Express Polym Lett*. 2011;5(8):742–52.
59. Nanaki S, Papageorgiou G, Bikiaris D. Crystallization of novel poly( $\epsilon$ -caprolactone)- block-poly(propylene adipate) copolymers. *J Therm Anal Calorim*. 2012;108(2):633–45.
60. Cesur S, Alp B, Küçüköksel Y, Kahraman T, Balköse D. Crystallization kinetics and affecting parameters on polycaprolactone composites with inorganic and organic additives. *J Vinyl Addit Technol*. 2014;21(3):174–82.
61. Sattari M, Mirsalehi SA, Khavandi A, Alizadeh O, Naimi-Jamal MR. Non-isothermal melting and crystallization behavior of UHMWPE/SCF/nano-SiO<sub>2</sub> hybrid composites. *J Therm Anal Calorim*. 2015;122(3):1319–30.
62. Wu T-M, Chen E-C. Isothermal and nonisothermal crystallization kinetics of poly( $\epsilon$ -caprolactone)/multi-walled carbon nanotube composites. *Polym Eng Sci*. 2006;46(9):1309–17.
63. Wang X-L, Huang F-Y, Zhou Y, Wang Y-Z. Nonisothermal crystallization kinetics of poly( $\epsilon$ -caprolactone)/montmorillonite nanocomposites. *J Macromol Sci Part B*. 2009;48(4):710–22.
64. Wei Z, Yu F, Chen G, Qu C, Wang P, Zhang W, et al. Non-isothermal crystallization and melting behavior of poly( $\epsilon$ -caprolactone)-b-poly(ethylene glycol)-b-poly( $\epsilon$ -caprolactone) by DSC analysis. *J Appl Polym Sci*. 2009;114(2):1133–40.
65. Heo S-J, Kim S-E, Wei J, Hyun Y-T, Yun H-S, Kim D-H, et al. Fabrication and characterization of novel nano- and micro-HA/PCL composite scaffolds using a modified rapid prototyping process. *J Biomed Mater Res, Part A*. 2009;89A(1):108–16.
66. Dziadek M, Pawlik J, Menaszek E, Stodolak-Zych E, Cholewa-Kowalska K. Effect of the preparation methods on architecture, crystallinity, hydrolytic degradation, bioactivity, and biocompatibility of PCL/bioglass composite scaffolds. *J Biomed Mater Res B Appl Biomater*. 2015;103(8):1580–93.
67. Carmona VB, de Campos A, Marconcini JM, Mattoso LHC. Kinetics of thermal degradation applied to biocomposites with TPS, PCL and sisal fibers by non-isothermal procedures. *J Therm Anal Calorim*. 2014;115(1):153–60.